Romantic Story or Raman Scattering? Rose Petals as Ecofriendly, Low-Cost Substrates for Ultrasensitive Surface-Enhanced Raman Scattering

Sin-Yi Chou, Chen-Chieh Yu, Yu-Ting Yen, Keng-Te Lin, Hsuen-Li Chen,* and Wei-Fang Su

Department of Materials Science and Engineering, National Taiwan University, Number 1, Section 4, Roosevelt Road, Taipei, 10617 Taiwan (R.O.C.)

Ⓢ *Supporting Information*

ABSTRACT: In this Article, we present a facile approach for the preparation of ecofriendly substrates, based on common rose petals, for ultrasensitive surface-enhanced Raman scattering (SERS). The hydrophobic concentrating effect of the rose petals allows us to concentrate metal nanoparticle (NP) *aggregates* and analytes onto their surfaces. From a systematic investigation of the SERS performance when using upper and lower epidermises as substrates, we find that the lower epidermis, with its quasi-three-dimensional (quasi-3D) nanofold structure, is the superior biotemplate for SERS applications. The metal NPs and analytes are both closely packed in the quasi-3D structure of the lower epidermis, thereby enhancing the Raman signals dramatically within the depth of focus (DOF) of the Raman optical system. We have also found the effect of the pigment of the petals on the SERS performance. With the novel petal-based substrate, the SERS measurements reveal a detection limit for rhodamine 6G below the femtomolar regime (10^{-15} M), with high reproducibility. Moreover, when we employ an upside-down drying process, the unique effect of the Wenzal state of the hydrophobic petal surface further concentrate the analytes and enhanced the SERS signals. Rose petals are green, natural materials that appear to have great potential for use in biosensors and biophotonics.
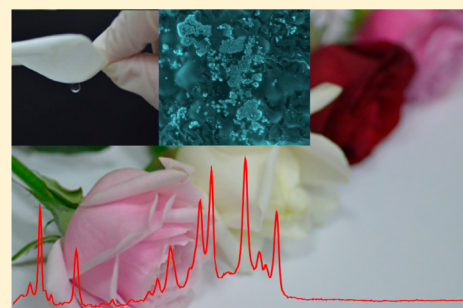
Raman scattering spectroscopy is a nondestructive and versatile analytical tool that provides characteristic vibrational, chemical, and structural information about a molecule. Surface-enhanced Raman scattering (SERS), a technique for increasing the intensity of Raman signals, has drawn much attention in various research fields.[1−4] There are two mechanisms that contribute to the SERS enhancement.[1] One is chemical enhancement, based on charge transfer between the analytes and the SERS substrate; the other, more-dominant mode of SERS enhancement is electromagnetic enhancement. When analytes are adsorbed on plasmonic nanostructures, the strong localized electric field (hot spots) that is generated can greatly enhance their Raman signals. Typically, plasmonic nanostructures are fabricated using complicated processes, such as focused ion beam and electron beam lithography and photolithography. To achieve a large electromagnetic field, plasmonic nanostructures or configurations have been designed to feature, for example, bow-tie antennas,[5,6] nanofocusing plasmonic waveguides,[7,8] and nanoscale metallic tips.[9,10] Although these nanostructures can provide strong electromagnetic fields, they have several shortcomings. First, the densities of the hot spots on these plasmonic nanostructures can be relatively low. As a result, such plasmonic nanostructures can enhance SERS signals only when the analytes are located precisely near the hot spots; typically, however, it is difficult to control the locations of analytes. Second, time-consuming,

expensive, low-throughput fabrication processes can result in these nanostructures being impractical for real-life detection.

The natural world has long fascinated people with its abundant, versatile, and functional structures and materials. For example, photonic crystal structures give butterfly wings their vibrant colors;[11,12] micro- and nanostructures result in lotus leaves being superhydrophobic;[13,14] and hierarchical fibrillar structures provide geckos with feet that exhibit excellent adhesion to any surface.[15,16] Replicating such biotemplates has allowed the simple fabrication of specific plasmonic structures. For example, Tan et al. used selective surface functionalization and subsequent electroless deposition to generate metallic replicas of the hierarchical submicrometer structures of butterfly wings; these unique metallic structures acted as SERS substrates for rhodamine 6G (R6G), with a limit of detection (LOD) as low as 10^{-13} M.[17,18] In contrast, Mu et al. developed an in situ synthesis method to form Au NPs on the 3D photonic architectures of butterfly wings, obtaining SERS substrates that demonstrated an LOD of 10^{-9} M for 4-aminothiophenol (4-ATP).[19] Likewise, Payne et al. used diatom frustules as sacrificial biotemplates to fabricate Au microshells, which, when used as SERS substrates, provided an LOD of 10^{-7} M for R6G.[20] Although versatile SERS substrates have been

proposed on biotemplates[21] or by replicating the nanostructures of biotemplates,[17−20] these SERS substrates have not utilized the intrinsic physical, chemical, or optical properties of the biotemplates themselves.

In addition to the presence of strong electromagnetic fields, the concentration of analytes can enhance the Raman signals as well.[22−24] When a droplet of an aqueous solution is placed on a hydrophobic surface, the droplet will maintain a spherical shape, with its solutes being concentrated during evaporation of the solvent, causing the residual solutes to be highly concentrated in a very small spot. This hydrophobic concentrating effect can allow the detection of trace amounts of analytes. Gentile et al. demonstrated a highly efficient SERS substrate based on artificial superhydrophobic structures decorated with Ag nanoclusters;[22−24] because these superhydrophobic structures concentrated solutes through the hydrophobic concentrating effect, the analytes were confined to a specific region, thereby enhancing the detection efficiency with an LOD as low as 10^{-18} M. Using this concept, several hydrophobic SERS substrates have been developed previously, including those based on Si micropillars,[22−24] ZnO nanowires,[25] and Teflon films.[26] These materials have, however, been fabricated artificially using complicated and expensive processes, again limiting their potential commercial applications for practical, real-life sensing. Nevertheless, there are many naturally accessible hydrophobic substrates, such as lotus leaves,[13,14] butterfly wings,[27,28] and rose petals.[29,30] Although Xu et al. proposed the use of hydrophobic rose petals as SERS substrates,[31] employing physical vapor deposition (PVD) to coat Ag films onto dried rose petals and, thereby, generate plasmonic hot spots, their approach has several drawbacks. First, a vacuum system is required to produce the metal nanostructures, thereby necessitating the use of dried rose petals as templates. Second, the electric field enhancement was not obvious on their SERS substrate, providing LODs as low as only 10^{-9} M.

In this study, we developed a facile solution-based process for the fabrication of highly sensitive SERS substrates on rose petals. Taking advantage of the hydrophobic concentrating effect, we found that NP suspensions and analytes were concentrated directly on fresh rose petals. Compared with other expensive hydrophobic SERS substrates prepared using complicated lithographic methods, these green substrates and the solution processes used in this study are considerably simpler and much more inexpensive. We have fully investigated the effects of the surface properties, material properties, and pigments of the rose petals on their SERS behavior. Our optimized rose petal−based SERS substrates provided lower LODs, with high reproducibility, relative to those of previously reported biological SERS substrates.

■ EXPERIMENTAL SECTION

Fabrication of SERS Substrates. Fresh roses of various colors were obtained commercially. A 20-μL droplet (7.4 × 10^{10} particles/mL) of a suspension of 100 nm Ag NPs (Ted Pella) was placed on the UE or LE of a clean rose petal, and allowed to dry. A 20-μL droplet of R6G (Sigma−Aldrich) was then placed on the NP-decorated petal and allowed to dry again.

Characterization. The morphologies of the samples were observed using an environmental scanning electron microscope (FEI-Quanta 200F). CAs were measured using a CA meter (Sindatek Model 100SB).

SERS. SERS spectra were recorded using a confocal Raman microscope (WITec, CRM200) equipped with a polarizer at an excitation wavelength of 632.8 nm (He−Ne laser) and a power of 34 mW. A 10× objective lens (NA = 0.25) was used; the signal integration time was 5 s.

■ RESULTS AND DISCUSSION

Figure 1a presents a photograph of some fresh roses having various vibrant colors. In general, the surface of a plant's petal
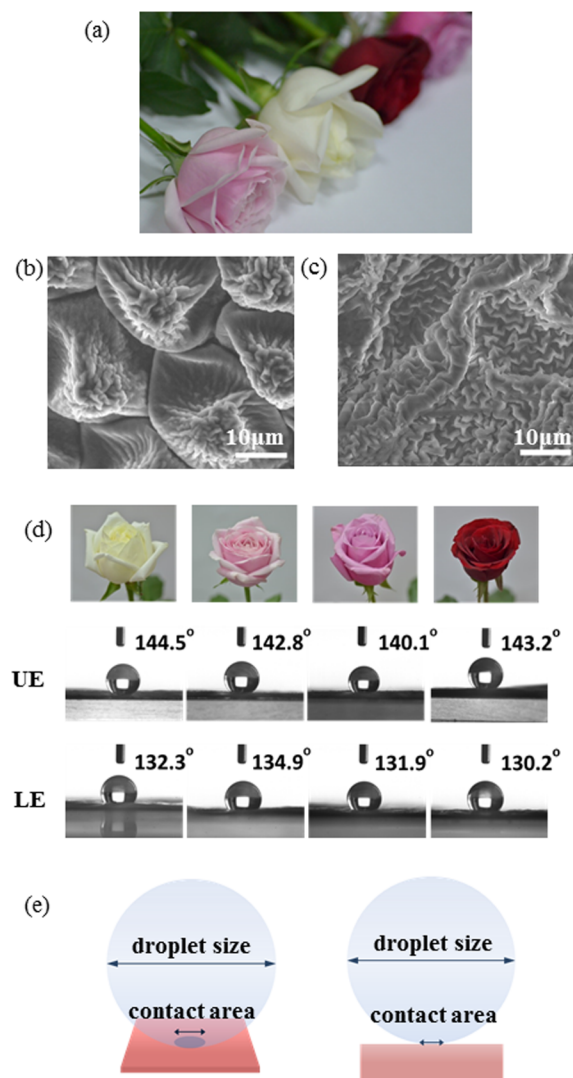
Figure 1. (a) Photograph of rose petals of various vibrant colors. (b, c) SEM images of the (b) UE and (c) LE of a rose petal. (d) CAs of the UE and LE of white, pink, deep pink, and red rose petals. (e) Schematic representation of a droplet on a hydrophobic rose petal, revealing that the contact area is much smaller than the droplet size because of the large CA.

features upper epidermis (UE) and lower epidermis (LE) tissues. Figures 1b and 1c display SEM images of the UE and LE, respectively, of a rose petal [Note that the morphologies of UE and LE on different colored rose petals are similar, which can be perceived from the SEM images (Supporting Information Figure S1)]; the two epidermises possess distinct morphologies. The UE comprises hierarchical micro- and nanostructures, with micropapillae arrays featuring nanofolds distributed throughout its surface. Such micropapillae arrays are

absent on the LE, which features only nanofolds. We suspected that the distinct morphologies of the UE and LE would result in different hydrophobic properties. Figure 1d presents the contact angles (CAs) of the UE and LE of rose petals of four different colors. Because the morphologies of the UEs of these various rose petals were all similar, their CAs were also similar (>140°), suggesting that the hydrophobic properties were nearly independent of the color of the roses tested in this study. On the other hand, the LEs possessed structures solely comprised of nanofolds, meaning that their CAs were slightly lower (~130°), but nevertheless revealing that their surfaces were also hydrophobic. The CAs suggested that both the UEs and LEs had good hydrophobicities. The large CAs resulted in small contact areas between water droplets and the hydrophobic petals (Figure 1e). Therefore, any suspended NPs or dissolved analytes in a droplet would be concentrated into a small spot (contact area) upon evaporation. Accordingly, we tested the ability of both the UEs and LEs of rose petals to concentrate NPs and analytes through the hydrophobic concentrating effect.

Figure 2a illustrates the experimental process of concentrating NPs and analytes on a rose petal through the hydrophobic concentrating effect. First, we placed a 20-μL droplet of a 100 nm Ag NP suspension on a clean rose petal. Because the surface of the rose petal was hydrophobic, the droplet did not spread out and maintained its spherical shape. The contact area between the droplet and the petal was much smaller that the size of the droplet. When the Ag NP suspension gradually dried, the Ag NPs aggregated into a small spot, providing a high-density NP array. Next, we placed a drop of the analyte (in this case, R6G) onto the NP array and allowed it to dry. The analytes concentrated during the drying process and adsorbed onto the high-density NP array. As a result, the intensities of the SERS signals of the analyte increased dramatically. Figure 2b displays the photographic images of a rose petal (here, using its LE as an example) at each of the experimental steps. The resulting small spot confirmed that the rose petal had a hydrophobic concentrating effect for both the Ag NPs and the analyte (R6G) molecules. Because the UEs and LEs both provided CAs greater than 130°, each surface displayed a hydrophobic concentrating effect. After drying the drops of the NPs and the analytes, we recorded SEM images of the morphologies of the UE and LE (Figures 2c and 2d, respectively). On the UE, the aggregated NPs were distributed over the hierarchical micropapillae structures. Because the LE possessed a relatively planar structure (nanofolds only), the NPs on its surface were distributed much uniformly and randomly. Supporting Information Figure S2 presents the detailed morphologies of the UE and LE after each drying step.

Because the morphologies of the UEs and LEs of rose petals of various colors were similar, their distributions of NPs were nearly identical. Nevertheless, the vibrant colors of these roses originate from the pigments in their petals, suggesting that rose petals of different colors would display dissimilar SERS properties because of these various pigments. We measured the background Raman signals of blank rose petals of four different colors (white, pink, deep pink, red). Generally, background signals can interfere significantly with the SERS signals of analytes; therefore, it is desirable to eliminate background signals from the substrates, impurities, and even the analytes themselves.[32−34] Figure 3a reveals that the background signals were lowest on the white rose petals, whereas the red ones provided the greatest noise. Figure 3b
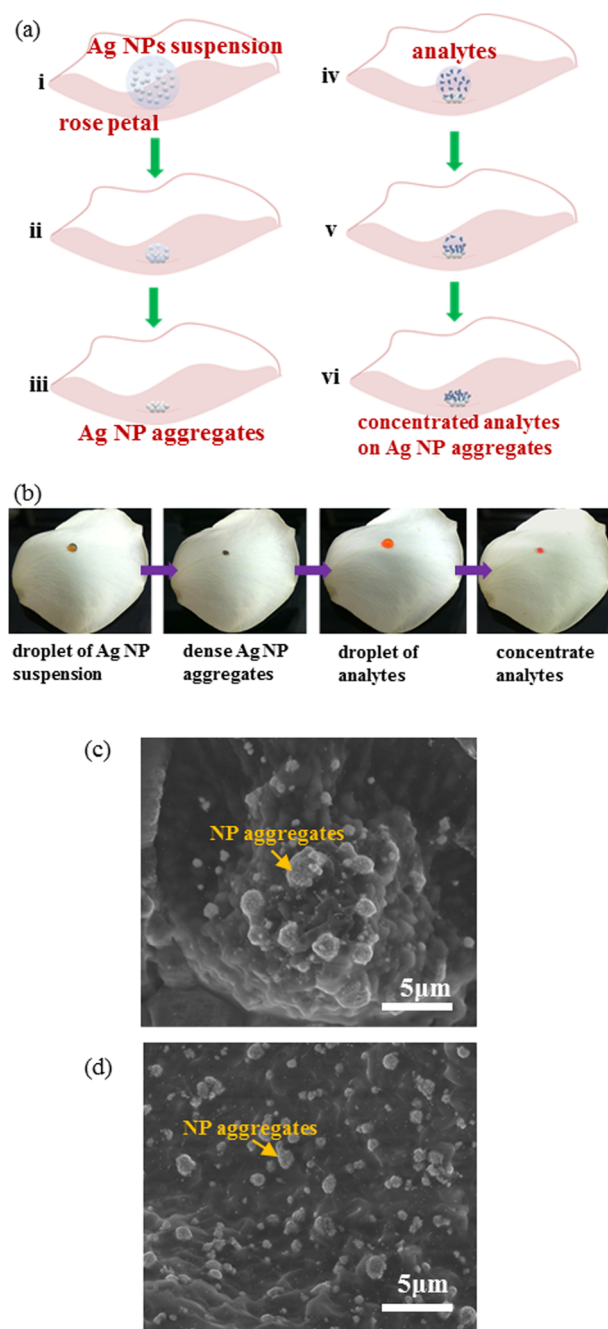
Figure 2. (a) Schematic representation and (b) photographic images of the process flow of concentrating Ag NPs and analytes on a rose petal. (c, d) SEM images of NP-decorated (c) UE and (d) LE after the analyte (R6G) had been concentrated on top of them.

displays the SERS spectra of R6G recorded after concentrating the NPs and R6G on the UEs of rose petals of the four different colors. The SERS signals were most intense when using the NP-decorated UE of a white rose petal as the substrate; the signals from a corresponding red petal were relatively weak. Therefore, pigments in rose petals can contribute a significant amount of background noise that might hinder detection of the signals of the analyte. Typically, pigments are contained in the mesophyll tissues sandwiched between the UE and LE.[35] Therefore, we attempted to eliminate the influence of any pigments, while maintaining the hydrophobicity of the surfaces, by peeling the UEs and LEs from the mesophyll tissues. Figures
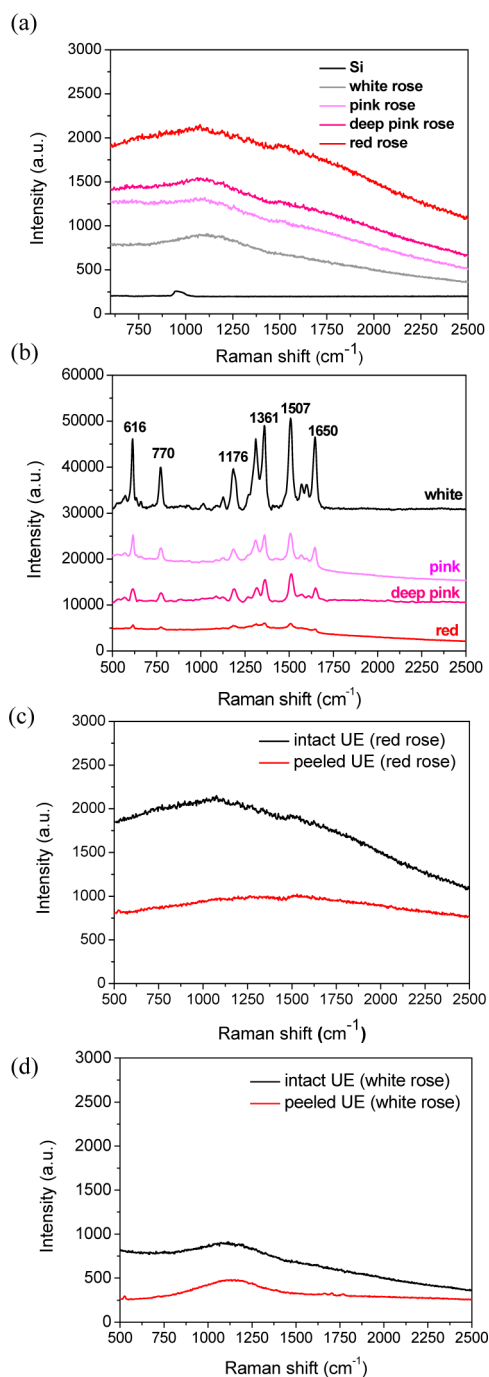
Figure 3. Raman spectra of (a) blank rose petals of various colors, (b) 10^{-6} M R6G concentrated on the NP-decorated UEs of rose petals of various colors, and (c, d) the blank intact UE and the peeled UE of a (c) red and (d) white rose petal. Note that the Raman spectra in panel b are offset by adding background to clearly show the Raman lines of R6G.

3c and 3d display the background Raman signals of the intact UEs and UEs peeled from the mesophyll tissues (so-called "peeled UEs") of red and white rose petals, respectively. The background signals of the UE of a red rose petal (Figure 3c) decreased significantly after the UE had been peeled from the mesophyll tissues. In addition, the background signals from the UE of a white rose petal, which contained relatively little pigment, was also further reduced after peeling (Figure 3d).

Next, we examined the morphologies of the peeled UE and peeled LE of a white rose petal. For the peeled UE, losing the support from the underlying tissues led to collapse and shrinkage of the micropapillae (Figure 4a); the CA decreased
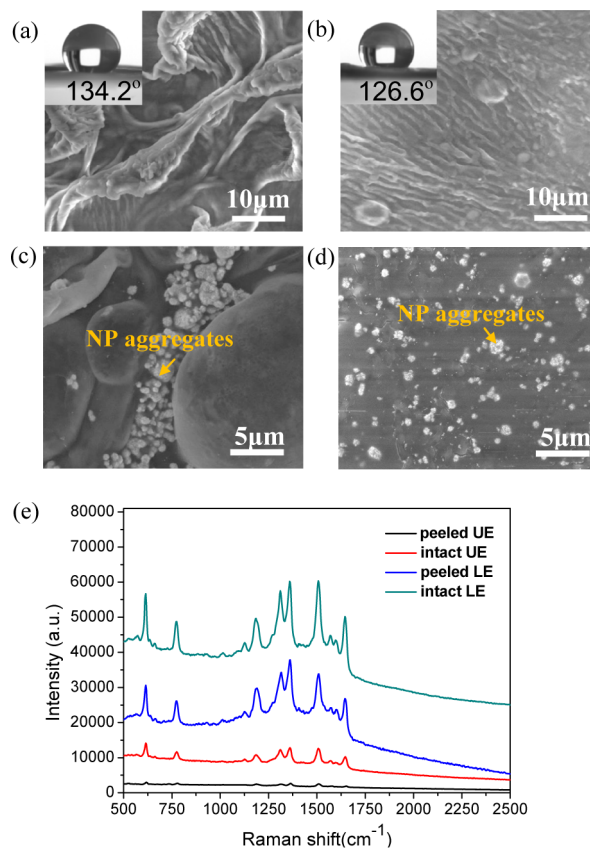
Figure 4. (a−d) SEM images of the blank (a) peeled UE and (b) peeled LE and NP-decorated (c) peeled UE and (d) peeled LE of a white rose petal. In panels c and d, the analytes had already been concentrated on the epidermises. (e) SERS spectra of 10^{-6} M R6G dried on the NP-decorated epidermises. Insets to panels a and b: Photographs of droplets with corresponding CAs.

from 140 to 134° as a result of the collapse of the hydrophobic structure. Similarly, a slight collapse of the nanofolds occurred on the peeled LE (Figure 4b), with its CA decreasing from 130 to 127°. Because the failure of the hydrophobic structure was not as dramatic on the peeled LE, its CA decreased relatively slightly. Notably, although the CAs of the UE and LE both decreased after peeling from the mesophyll tissues, the surfaces of the peeled UE and peeled LE remained hydrophobic because their CAs were greater than 120°.

In addition to the pigments, the aggregation and distribution of the NPs on the UE and the LE also had a great influence on the SERS performance. Because the hydrophobic structures on the peeled UE and peeled LE had changed, we expected to observe different distributions of their aggregated NPs. The NP aggregates and the analytes were also concentrated on the peeled UE and peeled LE using the process depicted in Figure 2a. Figures 4c and 4d present the corresponding SEM images; Supporting Information Figure S2 provides detailed morphologies of the peeled UE and peeled LE after each drying step. Because of the collapse of the micropapillae structures on the peeled UE, the NPs aggregated into the wrinkles under the collapsed micropapillae structures. For the peeled LE, the slight

decrease in the hydrophobic properties caused the density and uniformity of the NP aggregates to be lower than those on the intact LE. The distinct morphologies of the aggregated NPs between the UE and the LE, as well as between their intact and peeled counterparts, led us to further examine the SERS performance in each case.

Here, we tested the SERS performance of the NP-decorated UE, LE, peeled UE, and peeled LE of white rose petals. The SERS spectra of R6G dried on these four substrates revealed that the NP-decorated intact LE provided the largest enhancements in SERS signals, followed by the peeled LE, the intact UE, and the peeled UE (Figure 4e). Interestingly, the SERS performance of the intact LE was superior to that of the intact UE. We suggest that the quasi-three-dimensional (quasi-3D) distribution of the NPs on the nanofolds of the intact LE was superior to the 3D arrangement of NPs on the hierarchical micropapillae structures of the intact UE (cf., Figures 2c and 2d) when enhancing the SERS behavior. In a SERS measurement, the depth of focus (DOF) is an important factor that can affect the efficiency of signal collection. The DOF of a microscope is the range of distances in object space for which object points are imaged with acceptable resolution relative to the focal plane. Therefore, Raman scattering within the DOF would lead to greater collection of photons and contribute the most to the measured intensity. The DOF can be estimated using the equation[36]

$$DOF = k_2 \frac{n\lambda}{NA^2} \qquad (1)$$

where k_2 is the system-related coefficient, n is the refractive index of the object space medium, λ is the incident wavelength, and NA is the numerical aperture of the objective lens. Typically, the DOF lies in the range from a few hundred nanometers to a few micrometers; any NPs and analytes located within the DOF would contribute most significantly to the SERS signals. The heights of the micropapillae were typically in the range from 10 to 25 μm;[29−31] thus, most of the NPs were distributed outside the range of the DOF, contributing relatively weak signals. On the other hand, the vertical distribution of NPs on the nanofolds was in the range from a few hundred nanometers to one or two micrometers,[29−31] such that the NPs could become efficient hot spots within the range of the DOF for generating strong SERS signals. Therefore, the SERS performance of the intact LE was better than that of the intact UE. Moreover, regardless of whether we used the UE or the LE, the intact structure induced larger SERS signals than did the peeled one because the distribution of NPs had the greater effect on the SERS performance, even though the peeled surfaces provided lower background signals. The NPs on the peeled UE aggregated into the wrinkles beneath the collapsed micropapillae structures, such that the NP aggregates were possibly hindered from interacting with the analytes, causing inefficient collection of the SERS signals excited within the NP aggregates. On the other hand, the NPs were distributed less densely on the peeled LE, causing the SERS performance of the peeled epidermis to be poorer than that of the intact LE. Taking together the effects of the surface properties and the pigment of the epidermis, we suspected that the intact LE of a white petal would be the best rose petal−based biotemplate for SERS applications.

As displayed in the Figure S3 of Supporting Information, we used the three-dimensional finite-difference time domain (3D-FDTD) method to simulate the electric field amplitudes of NPs distributed on a 2D planar surface, the quasi-3D nanofolds of the LE, and the 3D micropapillae arrays of the UE. On the basis of the simulated results, we suspected that NPs dried on the quasi-3D nanofolds of the LE would be the most efficient SERS substrate. The detailed discussion can be found in Supporting Information.

Next, using the intact LE of a white rose petal to concentrate NPs and analytes, we determined the LOD for R6G on the NP-decorated rose petal. To do so, we dried R6G (20 μL) at various concentrations on the intact LE of a white rose petal. Figure 5a displays the corresponding SERS spectra. The NP-decorated intact LE allowed highly sensitive SERS detection, with an LOD as low as 10^{-15} M. At such a concentration, there would be approximately 12 040 R6G molecules in a 20-μL droplet. After such a droplet had dried and concentrated into an area of approximately 3 mm^2, on average there would be less
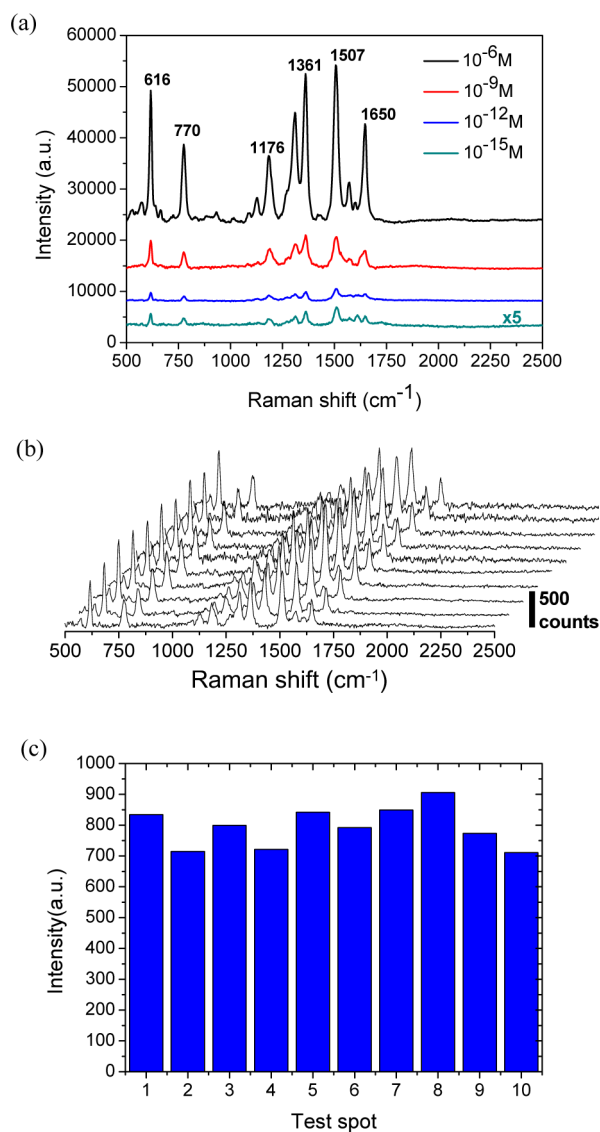
Figure 5. (a) Concentration-dependent SERS spectra of R6G that had been dried on the NP-decorated intact LE of a white rose petal. (b) Reproducibility of the SERS spectra of 10^{-12} M R6G collected at 10 randomly selected spots on the same NP-decorated intact LE. (c) Signal intensity of the 616 cm^{-1} line from R6G collected at 10 randomly selected spots on the same NP-decorated intact LE.

than one R6G molecule within the laser spot size (diameter = 3 μm). Accordingly, we suspect that the R6G molecules were not distributed uniformly within the drying spot. Therefore, a large area of NP aggregates was necessary to ensure that the trace analytes were located near hot spots. Compared with other reported SERS substrates and NP-decorated glass substrate (Supporting Information Figure S4), the large-area, dense NP aggregates on the rose petal provided a facile platform for the detection of trace amounts of R6G. According to our calculations, the detection of single molecules was almost possible on the NP-decorated intact LE. This high sensitivity originated from the quasi-3D distribution of NPs on the nanofolds of the intact LE.

Most of the NPs (hot spots) were positioned within the DOF, thereby contributing efficiently to the SERS enhancement. And the enhancement factor is calculated as above 10^9 (Supporting Information Figure S5). In addition to high sensitivity, the NP-decorated intact LE provided reproducible SERS signals. When we recorded the SERS spectra of 10^{-12} M R6G from 10 random spots within an area of 50 μm^2 (Figure 5b), the SERS signals were all of comparable intensity, suggesting that the SERS petal provided uniform SERS enhancements upon its entire surface. Furthermore, when we compared the intensities of the characteristic 616 cm^{-1} line of R6G in these 10 spectra (Figure 5c), the signal variations were less than 6%, suggesting outstanding reproducibility of the SERS signals enhanced by the rose petal-based SERS substrate. In addition, the high reproducibility can also be found across different dried spots on the same SERS petal (Supporting Information Figure S6).

In addition, we improved the SERS performance of the NP-decorated intact LE even further by taking advantage of the unique petal effect. Typically, the hydrophobicity of a rough surface can be divided into a Cassie−Baxter state and a Wenzel state.[37−39] In the Cassie−Baxter state, the liquid does not completely wet the rough surface because of air trapped between the rough solid surface and the liquid; in contrast, the Wenzel state involves homogeneous wetting of the rough surface. CA hysteresis is low in the Cassie−Baxter state, whereas it is large in the Wenzel state. The hydrophobicities of natural rough surfaces can be described using both models; two distinct effects have been observed: the lotus effect[13,14] and the petal effect.[29,30] The lotus effect describes a highly static CA with low CA hysteresis; a liquid droplet will readily move on such a surface while maintaining its spherical shape, as observed on lotus leaves. In contrast, the petal effect describes a surface exhibiting both a highly static CA and high CA hysteresis; in such a system, a liquid droplet will not roll off, even if the surface is turned upside down, as can occur on a rose petal. Therefore, we took advantages of the unique "petal effect" of rose petals to develop a highly efficient and sensitive SERS substrate.

Figure 6a and 6b reveals that a liquid droplet on a hydrophobic rose petal remains pinned to the surface without rolling off even when the petal is turned upside down. Therefore, we suspected a new approach for concentrating NPs and analytes would be to turn the petal upside down during the drying process. Under the effect of gravity,[40] the NPs and the analyte molecules would converge at the bottom of a droplet. As the solvent evaporated, the converged area would be much smaller than that on the top surface of the rose petal, leading to a higher concentration. Accordingly, the NP aggregates would be much denser if the droplet were to be dried upside down.
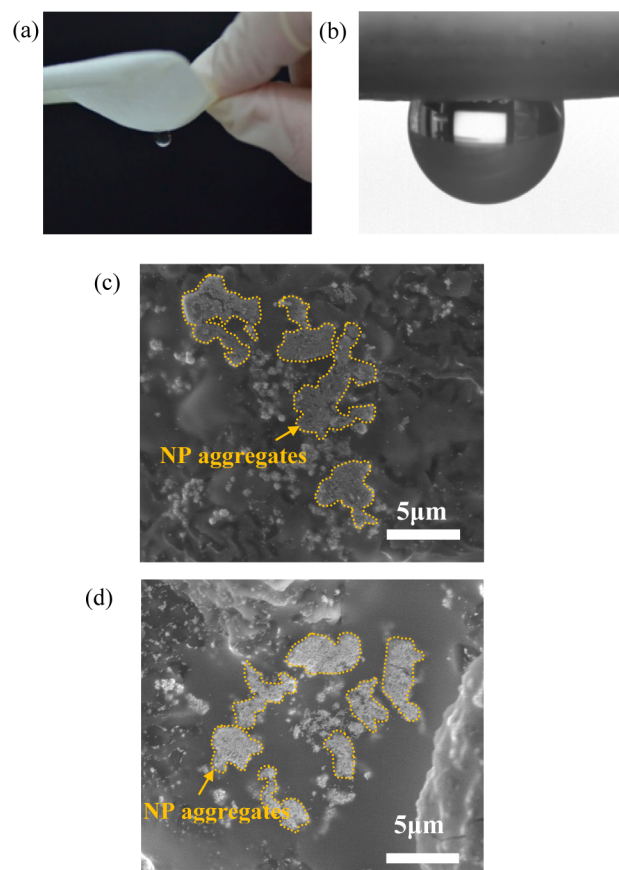
Figure 6. (a, b) Photographs of the petal effect of a rose petal. The water droplet did not roll off, even when the petal was turned upside down. (c, d) SEM images of NP aggregates concentrated on the intact LE through the upside-down drying process (c) before and (d) after an R6G droplet had been dried upon them.

Figure 6c and 6d present SEM images of NP aggregates concentrated on an intact LE when using the upside-down drying process; highly dense NP aggregates were present both before and after the analytes had dried on top of them, respectively. Compared with the NPs dried in the usual upward manner (Figure 2d), the NPs concentrated using the upside-down approach on an intact LE had a higher density and a more closely packed distribution. We suspected that strong coupling between such nearby NPs would further enhance the SERS signals. Therefore, we measured the SERS spectra of R6G dried upside down on the intact LE of a white rose petal (Figure 7a). Compared with the SERS spectra of the corresponding sample dried in the usual upward manner (Figure 5a), the SERS signals had greater intensity after drying upside down on the intact LE. Again, the detectable concentration readily reached down to 10^{-15} M. Figures 7b and 7c compare the peak intensities of the signals at 1361 and 1507 cm^{-1}, respectively, of R6G after drying upward and downward on the NP-decorated intact LE. Both Raman signals of R6G were enhanced when adopting upside down drying on the NP-decorated intact LE that possessed a higher density of NP aggregates. Figure 7d presents the corresponding enhancement ratios. After upside-down drying on an NP-decorated intact LE, the SERS signals of R6G were further enhanced approximately 2-fold at a concentration of 10^{-6} M; the enhancement ratios gradually decreased to approximately 1.1 times at a concentration of 10^{-15} M. The peak intensities for
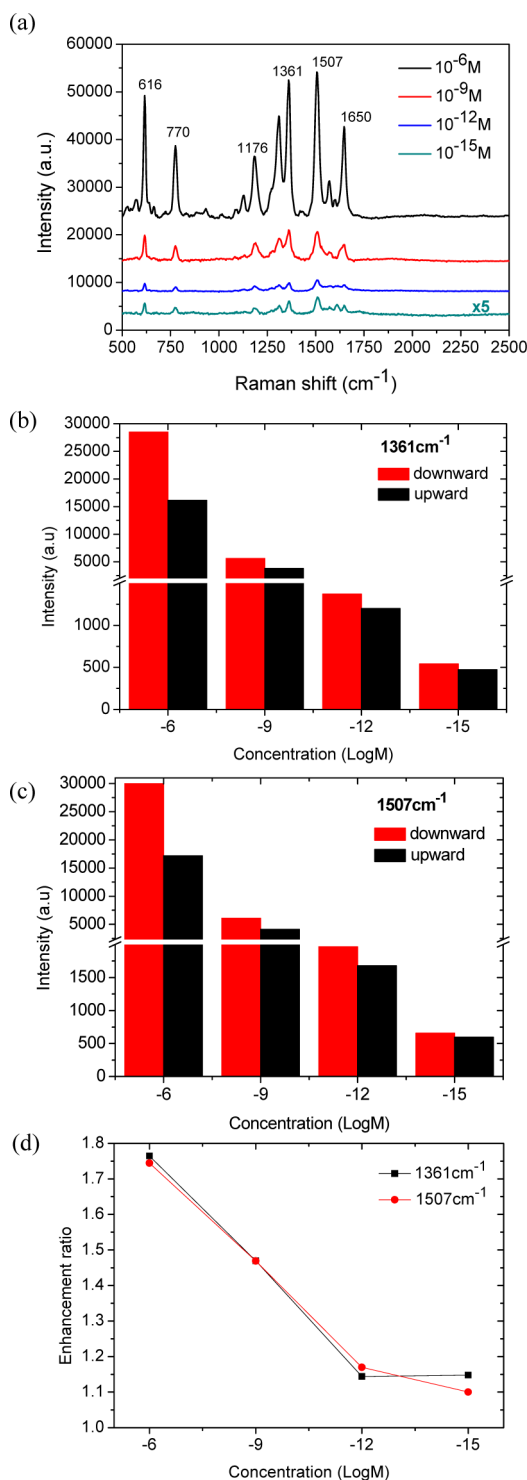
Figure 7. (a) Concentration-dependent SERS spectra of R6G dried on the upside-down−dried, NP-decorated intact LE of a white rose petal. (b, c) Peak intensities of the (b) 1361 and (c) 1507 cm^{-1} lines of R6G that had been dried upward and downward (upside-down) on the NP-decorated intact LE. (d) Enhancement ratios of the signals in panels b and c.

R6G at 10^{-15} M were relatively close because the SERS signals of R6G were all excited only in regions of highly dense NP aggregates at such a trace amount. Indeed, some NP clusters and highly dense NP aggregates were also present on the upwardly dried NP-decorated intact LE. At a high concen-

tration of R6G, all of these hot spots would contribute to the SERS signals; at a low concentration of 10^{-15} M, however, only those R6G molecules located near the highly dense NP aggregates would be observed, due to the larger electromagnetic enhancement at these positions. In contrast, large areas of highly dense NP aggregates were present on the upside-down−dried NP-decorated intact LE. Thus, the SERS signals of R6G would be excited and enhanced by these highly dense hot spots, regardless of the concentration of R6G.

CONCLUSIONS

In summary, we have developed eco-friendly, ultrasensitive SERS substrates based on hydrophobic rose petals. Because of a hydrophobic concentrating effect, Ag NPs and analyte molecules both underwent concentration and aggregation on the rose petals. The nanogaps between adjacent Ag NPs dramatically enhanced the electric field and, accordingly, the Raman signals. From investigations of the morphologies of the UEs and LEs of rose petals, we found that the quasi-3D distribution of NP *aggregates* on the LE contributed most efficiently to the SERS signals. Any effect of the pigments of the rose petals was eliminated after peeling the epidermis from the mesophyll tissues. By examining the morphologies and the distribution of NPs on the intact and peeled UEs and LEs, we confirmed that the intact LE of a white rose petal was the most sensitive and efficient SERS substrate. We achieved LODs as low as the femtomolar regime (10^{-15} M), with highly reproducible SERS signals. Moreover, taking advantage of the unique petal effect (Wenzal state) of the hydrophobic rose petal surface, we optimized the distribution of NPs on the intact LE through drying in an upside-down manner, thereby further enhancing the intensity of the SERS signals from the analyte and, accordingly, the sensitivity of the SERS process.

ASSOCIATED CONTENT

S **Supporting Information**

Complete SEM images of the UE and LE of different colored rose petals, the rose petals at each step of the drying process, additional discussions on the distribution of NPs and SERS performance by 3D-FDTD method, SERS performance of NP-decorated glass substrate, enhancement factor of the SERS petal, and reproducibility test across different dried spots on a SERS petal. The Supporting Information is available free of charge on the ACS Publications website at DOI: 10.1021/acs.analchem.5b00551.

AUTHOR INFORMATION

Corresponding Author

*E-mail: hsuenlichen@ntu.edu.tw.

Notes

The authors declare no competing financial interest.

REFERENCES

(1) Campion, A.; Kambhampati, P. *Chem. Soc. Rev.* **1998**, 27, 241−250.

(2) Greeneltch, N. G.; Davis, A. S.; Valley, N. A.; Casadio, F.; Schatz, G. C.; Van Duyne, R. P.; Shah, N. C. *J. Phys. Chem. A* **2012**, *116*, 11863−11869.

(3) Zhu, Y.; Kuang, H.; Xu, L.; Ma, W.; Peng, C.; Hua, Y.; Wang, L.; Xu, C. *J. Mater. Chem.* **2012**, *22*, 2387−2391.

(4) Ma, W.; Sun, M.; Xu, L.; Wang, L.; Kuang, H.; Xu, C. *Chem. Commun.* **2013**, *49*, 4989−4991.

(5) Hatab, N. A.; Hsueh, C. H.; Gaddis, A. L.; Retterer, S. T.; Li, J. H.; Eres, G.; Zhang, Z.; Gu, B. *Nano Lett.* **2010**, *10*, 4952−4955.

(6) Dodson, S.; Haggui, M.; Bachelot, R.; Plain, J.; Li, S.; Xiong, Q. *J. Phys. Chem. Lett.* **2013**, *4*, 496−501.

(7) Choo, H.; Kim, M. K.; Staffaroni, M.; Seok, T. J.; Bokor, J.; Cabrini, S.; Schuck, P. J.; Wu, M. C.; Yablonovitch, E. *Nat. Photonics* **2012**, *6*, 838−844.

(8) Verhagen, E.; Polman, A.; Kuipers, L. K. *Opt. Express* **2008**, *16*, 45−57.

(9) Berweger, S.; Atkin, J. M.; Olmon, R. L.; Raschke, M. B. *J. Phys. Chem. Lett.* **2012**, *3*, 945−952.

(10) van Schrojenstein Lantman, E. M.; Deckert-Gaudig, T.; Mank, A. J. G.; Deckert, V.; Weckhuysen, B. M. *Nat. Nanotechnol.* **2012**, *7*, 583−586.

(11) Biró, L. P.; Kertész, K.; Vértesy, Z.; Márk, G. I.; Bálint, Zs.; Lousse, V.; Vigneron, J. P. *Mater. Sci. Eng., C* **2007**, *27*, 941−946.

(12) Kertész, K.; Bálint, Zs.; Vértesy, Z.; Márk, G. I.; Lousse, V.; Vigneron, J. P. *Phys. Rev. E* **2006**, *74*, No. 021922.

(13) Barthlott, W.; Neinhuis, C. *Planta* **1997**, *202*, 1−8.

(14) Koch, K.; Bhushan, B.; Barthlott, W. *Soft Matter* **2008**, *4*, 1943−1963.

(15) Autumn, K.; Liang, Y. A.; Hsieh, S. T.; Zesch, W.; Chan, W. P.; Kenny, T. W.; Fearing, R.; Full, R. J. *Nature* **2000**, *405*, 681−685.

(16) Autumn, K.; Sitti, M.; Liang, Y. A.; Peattie, A. M.; Hansen, W. R.; Sponberg, S.; Kenny, T. W.; Fearing, R.; Israelachvili, J. N.; Full, R. J. *Proc. Natl. Acad. Sci. U.S.A.* **2002**, *99*, 12252−12256.

(17) Tan, Y.; Gu, J.; Xu, L.; Zang, X.; Liu, D.; Zhang, W.; Liu, Q.; Zhu, S.; Su, H.; Feng, C.; Fan, G.; Zhang, D. *Adv. Funct. Mater.* **2012**, *22*, 1578−1585.

(18) Tan, Y.; Gu, J.; Zang, X.; Xu, W.; Shi, K.; Xu, L.; Zhang, D. *Angew. Chem., Int. Ed.* **2011**, *50*, 8307−8311.

(19) Mu, Z.; Zhao, X.; Xie, Z.; Zhao, Y.; Zhong, Q.; Bo, L.; Gu, Z. *J. Mater. Chem. B* **2013**, *1*, 1607−1613.

(20) Payne, E. K.; Rosi, N. L.; Xue, C.; Mirkin, C. A. *Angew. Chem., Int. Ed.* **2005**, *44*, 5064−5067.

(21) Liu, X.; Zong, C.; Ai, K.; He, W.; Lu, L. *ACS Appl. Mater. Interfaces* **2012**, *4*, 6599−6608.

(22) De Angelis, F.; Gentile, F.; Mecarini, F.; Das, G.; Moretti, M.; Candeloro, P.; Coluccio, M. L.; Cojoc, G.; Accardo, A.; Liberale, C.; Zaccaria, R. P.; Perozziello, G.; Tirinato, L.; Toma, A.; Cuda, G.; Cingolani, R.; Di Fabrizio, E. *Nat. Photonics* **2011**, *5*, 682−687.

(23) Gentile, F.; Coluccio, M. L.; Accardo, A.; Marinaro, G.; Rondanina, E.; Santoriello, S.; Marras, S.; Das, G.; Tirinato, L.; Perozziello, G.; De Angelis, F.; Dorigoni, C.; Candeloro, P.; Di Fabrizio, E. *Microelectron. Eng.* **2012**, *97*, 349−352.

(24) Gentile, F.; Coluccio, M. L.; Coppede, N.; Mecarini, F.; Das, G.; Liberale, C.; Tirinato, L.; Leoncini, M.; Perozziello, G.; Candeloro, P.; De Angelis, F.; Di Fabrizio, E. *ACS Appl. Mater. Interfaces* **2012**, *4*, 3213−3224.

(25) Xu, F.; Zhang, Y.; Sun, Y.; Shi, Y.; Wen, Z.; Li, Z. *J. Phys. Chem. C* **2011**, *115*, 9977−9983.

(26) Lu, L. Q.; Zheng, Y.; Qu, W. G.; Yu, H. Q.; Xu, A. W. *J. Mater. Chem.* **2012**, *22*, 20986−20990.

(27) Ding, Y.; Xu, S.; Zhang, Y.; Wang, A. C.; Wang, M. H.; Xiu, Y.; Wong, C. P.; Wang, Z. L. *Nanotechnology* **2008**, *19*, 355708−1−355708−7.

(28) Goodwyn, P. P.; Maezono, Y.; Hosoda, N.; Fujisaki, K. *Naturwissenschaften* **2009**, *96*, 781−787.

(29) Feng, L.; Zhang, Y.; Xi, J.; Zhu, Y.; Wang, N.; Xia, F.; Jiang, L. *Langmuir* **2008**, *24*, 4114−4119.

(30) Bhushan, B.; Nosonovsky, M. *Philos. Trans. R. Soc. A* **2010**, *368*, 4713−4728.

(31) Xu, B. B.; Zhang, Y. L.; Zhang, W. Y.; Liu, X. Q.; Wang, J. N.; Zhang, X. L.; Zhang, D. D.; Jiang, H. B.; Zhang, R.; Sun, H. B. *Adv. Optical Mater.* **2013**, *1*, 56−60.

(32) Ikeda, K.; Suzuki, S.; Uosaki, K. *J. Am. Chem. Soc.* **2013**, *135*, 17387−17392.

(33) Nie, S.; Emory, S. R. *Science* **1997**, *275*, 1102−1106.

(34) Kagan, M. R.; McCreery, R. L. *Anal. Chem.* **1994**, *66*, 4159−4165.

(35) Inada, N.; Wildermuth, M. C. *Planta* **2005**, *221*, 9−16.

(36) Webb, R. H. *Rep. Prog. Phys.* **1996**, *59*, 427−471.

(37) Wenzel, R. N. *Ind. Eng. Chem.* **1936**, *28*, 988−994.

(38) Cassie, A. B. D.; Baxter, S. *Trans. Faraday Soc.* **1944**, *40*, 546−551.

(39) Callies, M.; Quéré, D. *Soft Matter* **2005**, *1*, 55−61.

(40) Keskin, S.; Çulha, M. *Analyst* **2012**, *137*, 2651−2657.